ACS OMEGA

Open Access

http://pubs.acs.org/journal/acsodf

Article

Improving Water Retention in Sandy Soils with High-Performance Superabsorbents Hydrogel Polymer

Haneen Omar and Edreese Alsharaeh*

Cite This: *ACS Omega* 2024, 9, 23531−23541

Read Online

ACCESS | Metrics & More | Article Recommendations

ABSTRACT: Improving the water retention capability of drained and sandy soils is vital for nurturing high-quality soil. This protective measure ensures the conservation of essential nutrients, such as fertilizers and organic matter; maintains soil quality; and prevents erosion. Superabsorbent hydrogels (SAHs) have emerged as promising solutions to boost water retention in sandy soils, typically characterized by a poor water-holding capacity. However, there is a noticeable gap in the existing literature regarding their potential to simultaneously achieve elevated swelling ratio (SR) and water retention ratio (WRR) levels. This study presents innovative SAH systems with the highest reported SR value yet, exceeding 10000 wt %, and remarkable WRR capability explicitly designed for agricultural use. These novel SAHs were synthesized using the chemical cross-linking polymerization method from polyacrylamide (PAM) polymer, employing various PAM ratios through a one-pot hydrothermal vessel method along with diverse drying techniques. The prepared hydrogels were characterized using various techniques, such as FTIR and DSC; unraveling insights into their structural properties; and the kinetics of the swelling process. Notably, these synthesized hydrogels exhibit robustness, maintaining structural integrity even under extreme conditions such as high temperatures or pressures. Our findings suggest immense potential for these hydrogels as soil enhancers in agriculture, offering a sustainable solution to bolster soil quality and nutrient preservation.

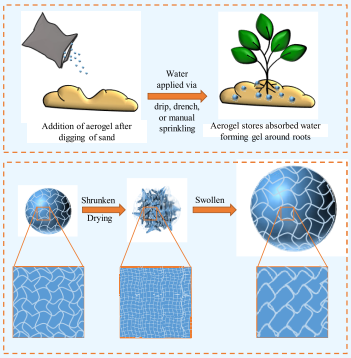

1. INTRODUCTION

Globally, the dramatic increase in the worldwide population in recent years raises concerns related to the food security crisis and water scarcity.[1,2] Projections indicate that, by 2050, with an expected population of 10 billion people, meeting their nutritional needs will require a substantial boost in agricultural output and a surge in water demand.[3] Therefore, ensuring a secure, safe, nutritious, and sustainable food supply becomes imperative for the well-being of future generations.

Traditional agricultural production often suffers from multiple constraints, including harsh climate, abiotic stresses (temperature, salinity, and drought), and shortage of water resources.[3,4] Key determinants of soil suitability for effective agricultural production lie in its water absorbency and retention capabilities.[5−7] Despite adequate rainfall or irrigation, the inadequate water storage capacity of soils can subject plants to water deficits.[8]

In spite of sandy soils having high water affinity, their primary drawback lies in inadequate water retention. Consequently, there is an ongoing demand for effective management strategies that minimize water seepage and enhance soil water storage. The utilization of soil conditioners has emerged as a prevalent and promising solution to enhance soil structure and address this issue.

Among various soil conditioners, hydrogels stand out as the most appealing materials in the agriculture industry. Due to their remarkable swelling properties and sustained release of absorbed molecules, they effectively function as a reservoir for water and essential substances in the root zone. In addition to their cost-effectiveness, stability when swollen, and significant contribution to soil remediation make them a highly sought-after solution.[4,9−11]

Superabsorbent hydrogels (SAHs) represent a unique class of hydrophilic polymers characterized by a robust three-dimensional structure. They can absorb and retain large quantities of water even under extreme environmental conditions such as heat or pressure, all without compromising their structural integrity. Their mechanical strength and elasticity can vary depending on the polymer composition and cross-linking density. They may become soft and gel-like when hydrated. Various polymerization approaches can be employed to synthesize SAHs,[12,13] including solution polymerization,[14] suspension polymerization,[15] inverse emulsion polymerization,[16] and cross-linking polymerization.[17]

These SAHs showed vast potential applications in various fields, such as hygiene products, agriculture, wound care, drug

Received: January 22, 2024
Revised: April 24, 2024
Accepted: April 26, 2024
Published: May 22, 2024

https://doi.org/10.1021/acsomega.4c00727
ACS Omega 2024, 9, 23531−23541

Table 1. Preparation Methods of the PAM Hydrogel with Different Ratios

Sample No.	Sample Name	Gel Formation	H_2O (mL)	PAM Solution (5 mL) PAM-4 st % (mg)	HQ (mg)	HMT (mg)	KCl-2 wt % (mg)	Curing Conditions
1	Low Mol. PAM-**15 wt** %-(30% OrgCL)	Gel	5	750	112.4	112.4	375	150 °C and 8 h
2	Low Mol. PAM-**30 wt** %-(30% OrgCL)	Gel	5	1500	224.9	224.9	750	150 °C and 8 h
3	Low Mol. PAM-**50 wt** %-(30% OrgCL)	Gel	5	2500	374.8	374.8	1250	150 °C and 8 h
4	Low Mol. PAM-**75 wt** %-(30% OrgCL)	Gel	5	3750	562.2	562.2	1875	150 °C and 8 h

delivery, and environmental remediation.[18−20] In the agriculture field, SAHs have found widespread use in enhancing the water retention capacity of sandy soils, enabling farming practices even in arid regions and desert environments.[21]

The vast majority of commercially available SAHs are synthetic polymers, predominantly derived from polyacrylamide (PAM) and acrylate.[22] These materials, marketed under names like "solid rain",[22] are prized for their biocompatibility, low toxicity, tunability, high stability, and remarkable water-absorption properties.[13,23]

The effectiveness and potential applications of SAHs depend on three main critical parameters: the swelling ratio (SR), swelling rate, and water retention ratio (WRR).

Despite the growing interest in SAHs for soil improvement applications, studies specifically addressing the optimization of SR and WRR in tandem are relatively scarce. Most research efforts have focused on either maximizing the SR or enhancing the WRR individually without fully exploring the synergistic effects that could result from optimizing both parameters simultaneously. For instance, Hong et al. employed γ radiation to synthesize a polysaccharide-based grafted sodium styrenesulfonate (SSS) SAH. This SAH exhibits SR 3230 g/g, while its WRR has not been reported.[24]

The highest SR and WRR results to date were published by Lv et al., reaching impressive figures of 5500 g/g and 60%, respectively. Their innovative SAH was produced by copolymerizing acrylic acid (AA) monomer and acrylic amide (AM) monomer, while utilizing calcium hydroxide ($Ca(OH)_2$) nanoparticles as a cross-linker.[25]

This research study aims to innovate SAH formulations with both high SR and remarkable WRR by using a simple polymerization process for agricultural and environmental applications.

Herein, we synthesized SAHs by varying the ratios of PAM hydrogel following a chemical cross-linking polymerization approach. This approach creates a 3D network structure within the hydrogel by forming covalent bonds between polymer chains. In this case, HQ and HMT serve as cross-linking agents, facilitating the cross-linking of the PAM chains to form the hydrogel network. KCl was added to control the ionic strength of the hydrogel and enhance its swelling capacity.

2. MATERIALS AND METHODS

2.1. Materials. Low molecular weight polyacrylamide (LMWPAM) (MW = 550000 g/mol) was obtained from the KSA. Hydroquinone (HQ) was purchased from Sigma-Aldrich (U.K.). Hexamethylenetetramine (HMT) and potassium chloride (KCl) were obtained from Loba Chemie.

2.2. Methods. Fourier transform infrared (FTIR) spectra were recorded by using a Thermo Scientific spectrometer (Nicolet iS10). Powder X-ray diffraction (XRD) measurements were performed using a Rigaku MiniFlex 600 instrument using Cu Kα radiation (40 V, 15 mA, λ = 1.54056 Å) in a θ−θ mode from 5° to 90° (2 θ). Differential scanning calorimetry (DSC) measurements were studied using Hitachi DSC7020 from −20 to 350 °C at a heating rate of 5 °C/min under a nitrogen flow of 50 mL/min. The thermogravimetric analysis (TGA) tests were carried out by PerkinElmer TGA 8000 thermogravimetric analyzer. The study was performed in an inert nitrogen atmosphere from 25 to 500 °C with a uniform heating rate of 5 °C/min. The nanotest 3 nanoindentation platform (product of Micromaterials, U.K.) was used to determine the samples' elastic modulus and hardness values. The load was measured as a function of the deformation depth. Berkovich-type diamond indenter was used with a maximum load of 20 mN. The experiment was done in the following sequence: (1) approaching the surface, (2) loading to the peak load of 20 mN at a rate of 5 mN/s, (3) holding the indenter at peak load for 30 s, and (4) unloading from the peak load at a rate of 20 mN/s. The holding step was included to eliminate the creep effect. Elastic modulus and hardness values were obtained through analysis using Nanotest software. Scanning electron microscopy (SEM) images were taken using a JEOL FE-SEM.

2.3. Preparation of Different PAM Hydrogels Using In Situ Method. *2.3.1. PAM-15 wt % Hydrogel.* A 750 mg amount of low molecular weight PAM was thoroughly mixed with 5 mL of deionized water and stirred for 1 h or until completely dissolved at room temperature. After that, 112.4 mg each of hydroquinone (HQ) and hexamethylenetetramine (HMT) alongside 375 mg of KCl salt were added to the PAM solution and further mixed for 15 min. Subsequently, the resultant solution was transferred into a hydrothermal vessel and placed in an oven set at 150 °C for 8 h.

The same preparation method was employed for PAM hydrogel with ratios of 30, 50, and 75 wt %, with varying PAM, HQ, HMT, and KCl weights, as shown in Table 1.

2.4. Water Absorption and Water Retention Experiments. To determine the water absorption capacity of various PAM hydrogels, portions of the hydrogels were subjected to drying processes: some in the oven and others in the freeze-dryer. Known weights of the gel form and oven-dried and freeze-dried hydrogels were submerged in an excess of deionized water. After a set duration, the swollen gels were extracted from the water and samples were weighed. The water absorption or swelling ratio (SR, wt %) at different temperatures was calculated using the following eq 1:

$$\mathrm{SR/(wt\ \%)} = \frac{\text{swollen weight} - \text{dried wieght}}{\text{dried weight}} \times 100 \quad (1)$$

To investigate the impact of temperature on SR (wt %), absorption studies were carried out at varying temperatures: 25, 50, and 80 °C.

The water retention experiment of PAM hydrogel measurements was conducted at 25 °C after the hydrogel reached its equilibrium swelling. This involved exposing the swollen hydrogel sample to the open air for different time intervals.

https://doi.org/10.1021/acsomega.4c00727
ACS Omega 2024, 9, 23531−23541

Scheme 1. Preparation of PAM Hydrogels with Different PAM Ratios Using Different Drying Methods

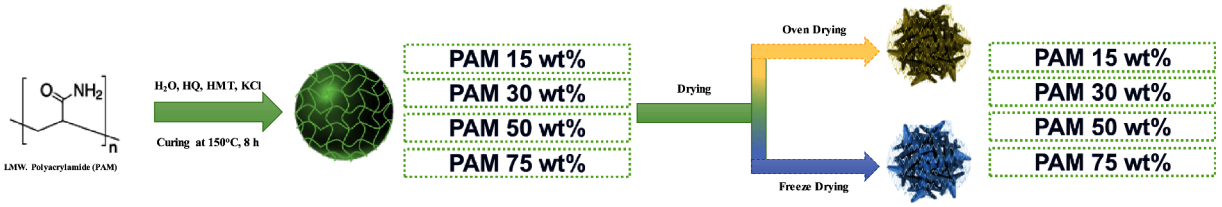

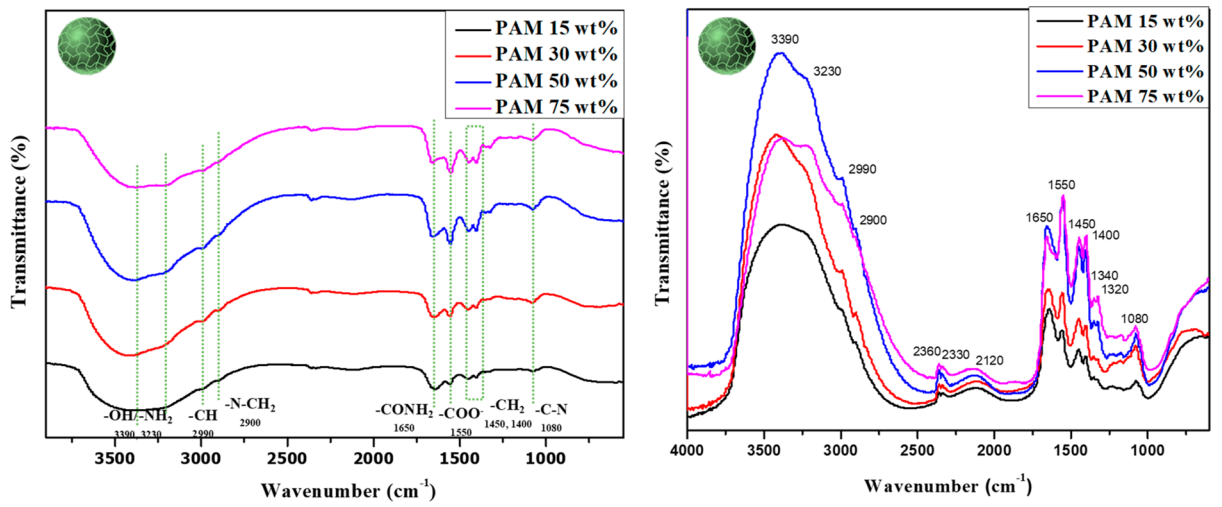

Figure 1. FTIR spectra of PAM hydrogels with different PAM ratios.

The water retention ratio (WRR) was determined using the following eq 2:

$$\mathrm{WRR}/\% = \frac{\text{dried wieght}}{\text{swollen weight}} \times 100 \quad (2)$$

2.5. Recyclability Experiment. The recyclability of the PAM hydrogel was assessed by immersing hydrogel samples of known weights in sufficient water to reach equilibrium and determining the swelling percentage using eq 1. Subsequently, the swollen samples were retrieved and oven-dried until they returned to their original weight. The swelling percentage for the dried hydrogel sample was measured again, following a similar procedure for a second cycle. This process was repeated multiple times to evaluate the samples' recycling potential.

3. RESULTS AND DISCUSSION

The selection of PAM hydrogels in this study was initially based on their excellent water absorption capacity, tunable properties, soil moisture retention abilities, and cost-effectiveness. These properties make them well-suited for addressing water scarcity, improving agricultural productivity, and promoting sustainable agricultural practices.[13,23]

PAM samples with distinct weight ratios were synthesized via the cross-linking polymerization method. Based on variations in polyacrylamide (PAM) concentrations and our previous study,[26] various formulation parameters have been systematically evaluated, in order to achieve optimal swelling capacity, mechanical strength, and stability. Varying the ratio of PAM to cross-linking agents (HQ and HMT) can impact the degree of cross-linking within the hydrogel network, thereby affecting its swelling behavior and absorption properties.

These hydrogels underwent drying via two methods: oven-drying and freeze-drying, resulting in the production of oven-dried hydrogels and aerogels, respectively. Eventually, the hydrogels were immersed in distilled water to investigate their swelling capacity and swelling mechanism at different temperatures (Scheme 1). Following this, the hydrogels' structural properties and thermal stability were analyzed using a range of techniques.

3.1. Fourier Transform Infrared (FTIR). In IR spectroscopy, the presence of different functional groups causes energy to be absorbed in certain wavelengths and retransmitted, generating distinct peaks. Figure 1 shows the FTIR spectra of the PAM hydrogels with different PAM ratios featuring all of the characteristic peaks. The broad transmittance bands observed at 3390 and 3230 cm^{-1} were assigned to (−OH stretching and $-NH_2$ asymmetric stretching) and secondary amide NH_2 stretching groups, respectively. Notably, distinctive peaks at 2990 and 2900 cm^{-1} were ascribed to asymmetric CH_2 groups and $-N-CH_2$ bonds. Additionally, the absorption bands at 1650 and 1550 cm^{-1} were attributed to primary amide C═O stretching ($CONH_2$) and secondary amide NH bending of the acrylamide unit. Furthermore, the transmittance bands observed at 1450 and 1080 cm^{-1} corresponded to $-CH_2$ and the stretching vibration of C−N groups, correspondingly.

3.2. X-ray Diffraction (XRD). XRD analysis was employed to examine the crystalline structure and phases within the PAM. Figure 2 exhibits the XRD patterns of PAM hydrogels with different PAM ratios. Across all samples, a broad diffraction peak around 26° represents the polymer's amorphous nature.

3.3. Differential Scanning Calorimetry (DSC). The stability and structure of PAM hydrogels are significantly influenced by both free and bound water. Free water pertains to water molecules bound together through hydrogen bonding,

https://doi.org/10.1021/acsomega.4c00727
ACS Omega 2024, 9, 23531−23541

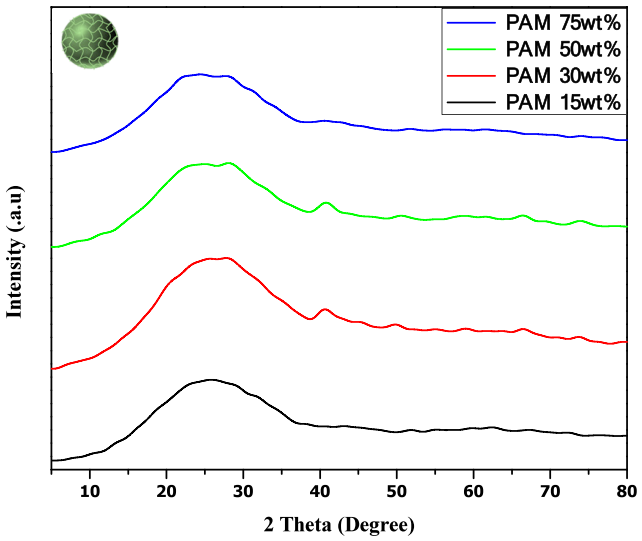

Figure 2. XRD patterns of PAM hydrogels with different PAM ratios.

while bound water specifically denotes water molecules chemically bound to the surface.

Equations 3 and 4 are applied to calculate the free and bound water in the hydrogel.

$$w_f = \frac{\Delta H}{\Delta H^\circ} \tag{3}$$

$$w_b = 1 - w_f \tag{4}$$

where w_b is the bound water, w_f is the free water, ΔH is the enthalpy required for heating the free water in the hydrogel, and ΔH° is the 333.5 J/g standard degradation enthalpy of free water.

Studying the thermal stability of the hydrogel requires understanding the interaction between the polymer and water molecules since the main abundant percentage of a hydrogel is water. In our observations, we noted that, at PAM concentrations of 30, 50, and 75% (wt %), the PAM hydrogel contained 100% bound water. In comparison, free water was present at a lower concentration of 15% (wt %), as illustrated in Figure 3. This suggests that higher PAM ratios result in a greater number of chemically bound or entrapped water molecules within the PAM matrix. Moreover, we observed a notable rise in the degradation temperature (T_{deg}) of PAM hydrogel by around 10 °C upon the increase of PAM percentage from 15 wt % up to 75 wt %. This rise was accompanied by increased degradation enthalpy (H_{deg}), indicating an enhanced gel strength. In other words, denser networks require higher energy to degrade due to increased cross-linking densities that restrict their chain mobility movements.

3.4. Thermogravimetric Analysis (TGA). Thermogravimetric analysis (TGA) was conducted to examine the results of various PAM ratios (15, 30, 50, and 75 wt %) and different drying methods of PAM-15 wt % (G, D, and A). The TGA curves for panels a and b in Figure 4 displayed a two-step weight loss for the PAM hydrogel.

In Figure 4a, the first step occurs. At temperatures below 100 °C, water molecules are removed through dehydration, resulting in a weight loss of the PAM sample. Figure 4a clearly shows a direct correlation between weight loss and PAM weight ratio percentages, as an increase in PAM weight ratio corresponds to a decrease in water molecules. The second step

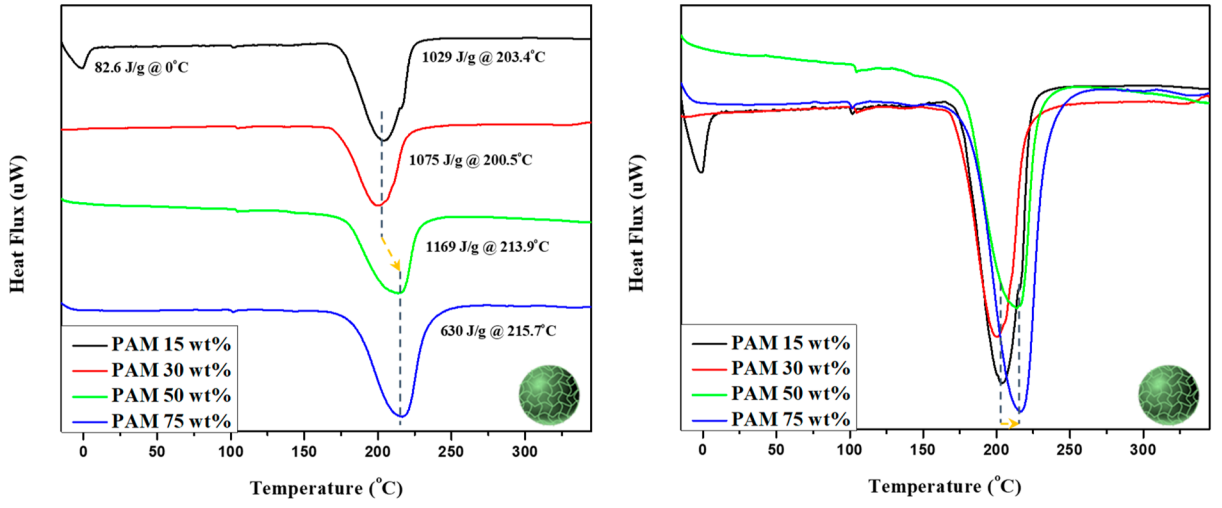

Sample No.	Sample Name	H_{water} (J/g)	w_f	w_b	H_{deg} (J/g)	T_{deg} (°C)
1	PAM 15 wt%	82.6	0.247676	0.752324	1029	203.4
2	PAM 30 wt%	-	0	1	1075	200.5
3	PAM 50 wt%	-	0	1	1169	213.9
4	PAM 75 wt%	-	0	1	630	215.7

Figure 3. DSC thermograms of PAM hydrogels with different PAM ratios.

https://doi.org/10.1021/acsomega.4c00727
ACS Omega 2024, 9, 23531−23541

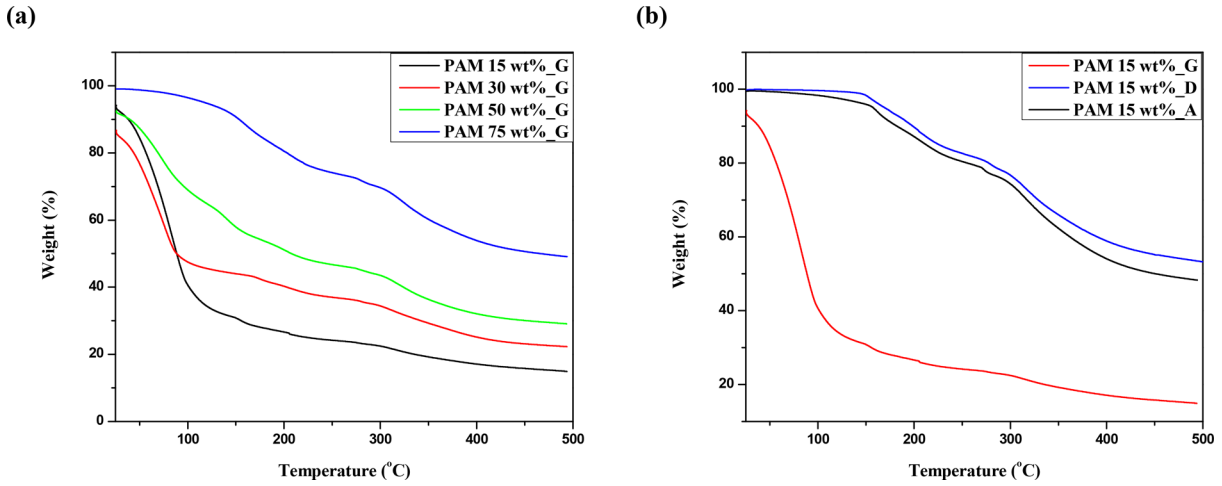

Figure 4. TGA curves of PAM hydrogels with different PAM ratios (a) and different drying methods of PAM-15 wt % (b).

	PAM 15% wt aerogel (MPa)
Elastic Modulus (MPa)	942
Hardness (MPa)	40.2

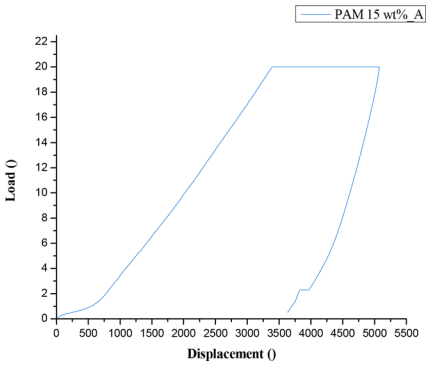

Figure 5. Load−displacement curve of PAM-15 wt % aerogel.

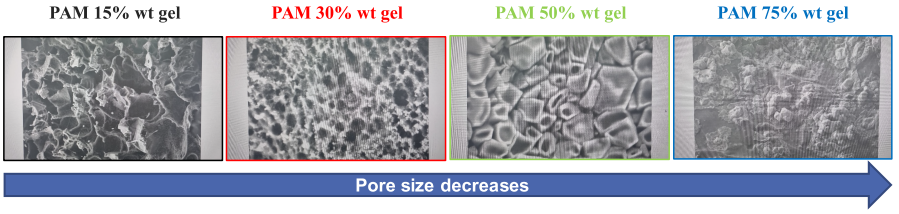

Figure 6. SEM images of PAM-15 wt % hydrogels with different PAM ratios.

occurs between 100 and 300 °C, corresponding to the thermal decomposition of the amide groups in PAM chains. Beyond 300 °C, the polymer chains fully decomposed and released NH_3, H_2O, and CO_2.[27−29] Generally, all samples exhibit similar behavior in terms of weight loss with increasing temperature despite variations in weight loss amounts.

The TGA curve was analyzed for PAM with a concentration of 15 wt % using various drying methods. (Figure 4b) When the temperature was below 100 °C, the PAM gel form displayed a primary weight loss caused by the evaporation of adsorbed water. Both the PAM-15 wt % samples labeled as D and A had minimal weight loss due to the drying process. Slight variations were observed in the degradation temperature of PAM-15 wt %_D and _A, 145 and 155 °C, respectively. This could be attributed to the formation of more rigid networks and higher degrees of cross-linking in PAM-15 wt %_A as opposed to PAM-15 wt %_D.

3.5. Mechanical Properties. The characteristics of PAM-15 wt % aerogel were analyzed using nanoindentation techniques, which have proven to be an effective way of measuring elastic mechanical properties when traditional tests are impractical. The aerogel was tested at multiple points, with 10 indents being averaged to determine the mean hardness (H) and elastic modulus (E) values.

The analysis results are presented in the table of Figure 5, indicating that PAM-15 wt % aerogel possesses remarkable mechanical strength. Furthermore, Figure 5 illustrates the load−displacement curve obtained during the nanoindentation experiment.

3.6. Scanning Electron Microscopy (SEM). A scanning electron microscope (SEM) was used to analyze the porosity of the synthesized PAM with different ratios and drying methods. Figure 6 illustrates how the PAM content significantly impacts the porosity structure of hydrogel, rising from 15 to 75 wt %. A denser network is observed at higher PAM content (PAM-75 wt %), indicating an inverse relationship between PAM content and porosity.

https://doi.org/10.1021/acsomega.4c00727
ACS Omega 2024, 9, 23531−23541

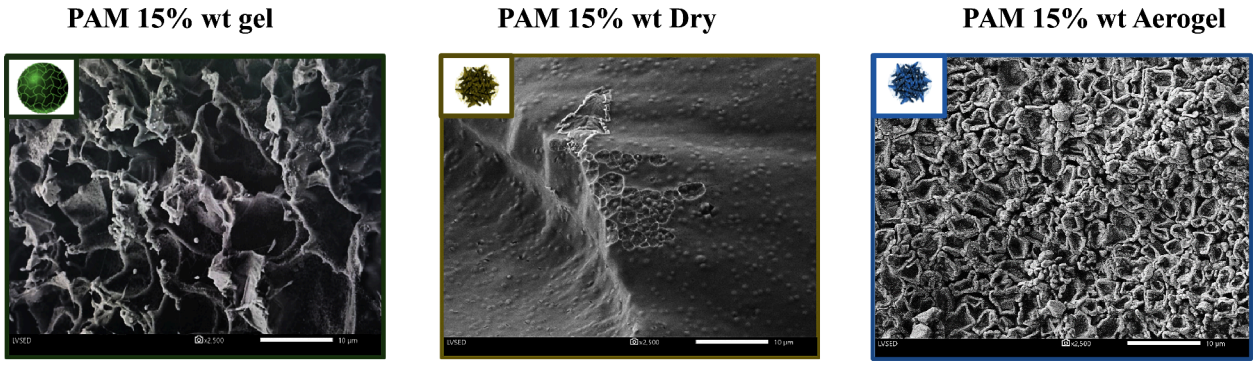

Figure 7. SEM images of PAM-15 wt % hydrogels at different drying methods.

Figure 7 shows the SEM images of PAM-15 wt % in its gel, dry, and aerogel forms. The gel form of PAM-15 wt % displays a network of porous structures with micropores. High-temperature evaporation during oven drying causes the structure to pack tightly, resulting in a nonporous structure (PAM-15 wt %_D). On the other hand, the freeze-drying method (PAM-15 wt %_A) produces porous structures with both micro- and nanopores. The extent of shrinkage determines the bulk sample density after drying, with the freeze-dried sample having the lowest bulk density due to its highly porous nature. The oven-dried structure had the highest bulk density because of its collapse during drying.

3.7. Swelling. Following physicochemical characterization, the potential of four different ratios of PAM hydrogels for soil water storage was assessed by examining key properties such as water absorption, swelling behavior, water retention, and recyclability.

To determine the SR of different PAM hydrogel ratios, gel-form samples were immersed in a water solution at room temperature and the water absorption rate was measured at different time intervals.

PAM hydrogel samples were cut into small pieces for the swelling studies by using a clean scissor (as depicted in Figure 8). They were subjected to a 48 h swelling study in distilled water at room temperature. Measurements were taken at 15 min intervals within the first hour and then hourly for the subsequent 3 h. Figure 9 illustrates the rapid increase in SR

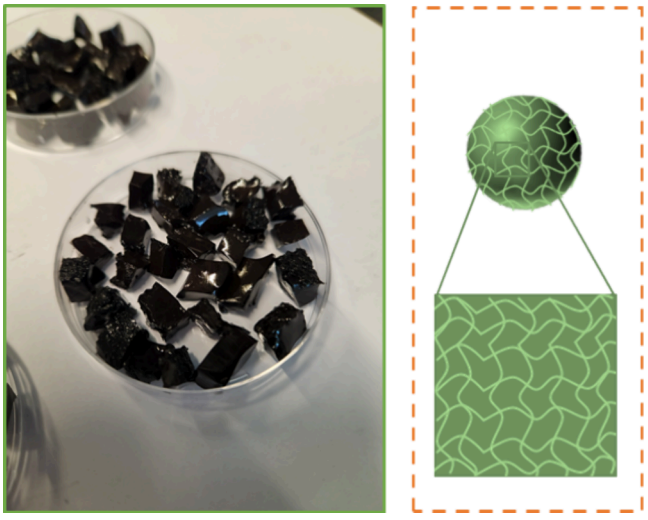

Figure 8. Small cut-it pieces of PAM hydrogels.

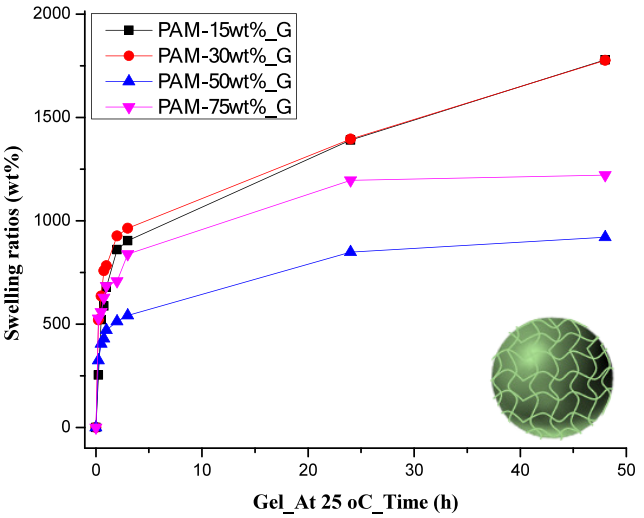

Figure 9. Water absorption of PAM hydrogels with different PAM ratios.

within the initial three h, reaching 50% of their equilibrium swelling rate. This was followed by a gradual increase until a plateau was reached. Notably, the PAM-15 wt % and PAM-30 wt % samples displayed the maximum absorption, achieving an SR of 1779 wt %.

The gels underwent drying using two distinct methods, thermal drying (oven drying) and nonthermal drying (freeze-drying) methods, to investigate their impact on water absorption capacity. As elucidated in Figure 10, particularly in the case of the freeze-dried (aerogel) samples, notably the PAM-15 wt %, a higher swelling ratio and faster water absorption rate were observed compared to the gel and oven-dried samples. This can be explained by the fact that capillary stress is avoided throughout the freeze-drying process, which prevents structural collapse and subsequently minimizes the shrinkage of the material. These results suggest that the freeze-drying method produces material with higher porosity, rigidity, and stable structure, which is a preferential path for water to penetrate. This was in contrast to the oven-dried samples, whose structures were entirely distorted.

Following the study on the impact of drying methods, it was found that the PAM hydrogel with a 15 wt % ratio exhibited the highest water absorption capacity, reaching an SR of around 8000 wt % in aerogel form at room temperature. As a result, we have decided to focus our current study specifically on the PAM-15 wt % ratio.

https://doi.org/10.1021/acsomega.4c00727
ACS Omega 2024, 9, 23531−23541

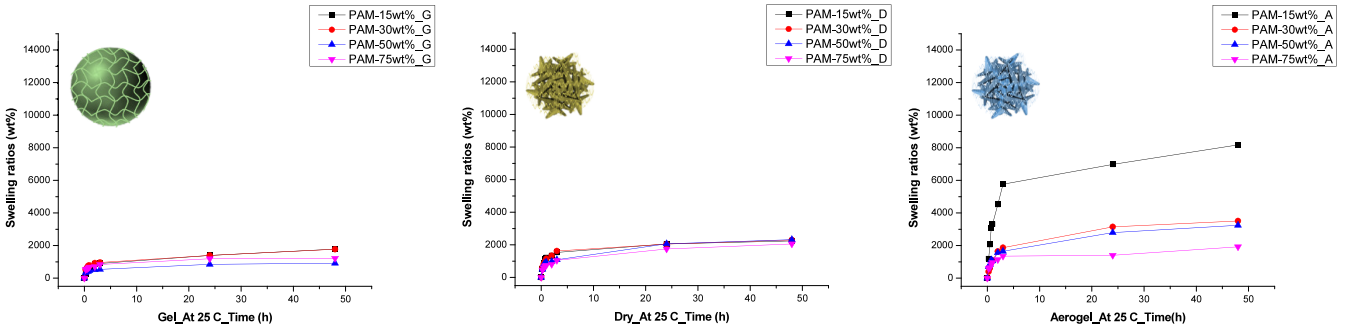

Figure 10. Water absorption of PAM hydrogels with different PAM ratios under different drying methods.

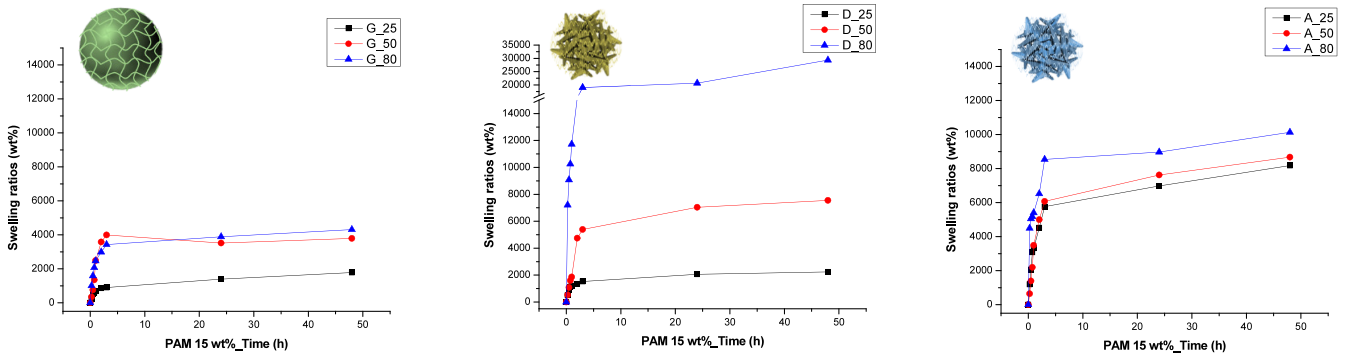

Figure 11. Water absorption of PAM-15 wt % ratios with different drying methods at different temperatures.

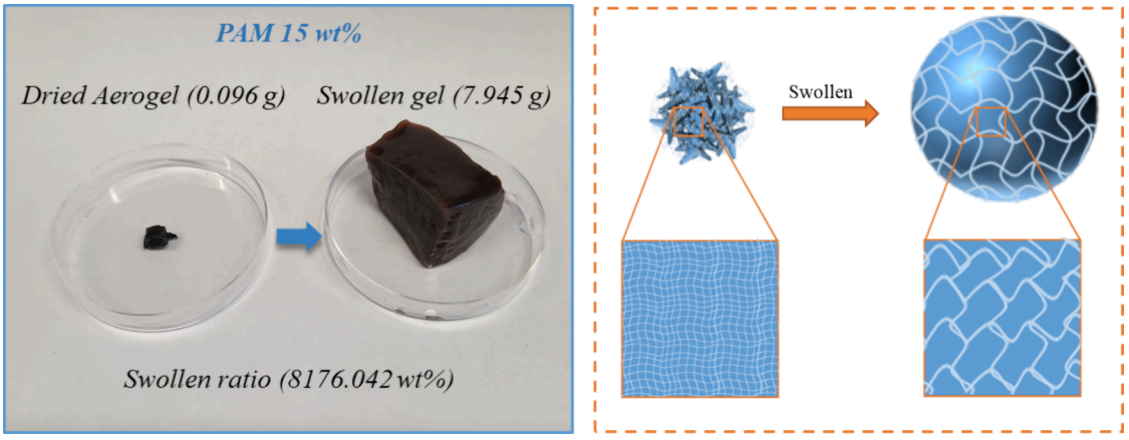

Figure 12. Picture of a small piece of 15 wt % PAM aerogel before and after being immersed into distilled water to acquire its equilibrium swelling at 25 °C.

Afterward, we investigated the effect of water-absorbing temperature (25, 50, and 80 °C) on the swelling ratio of PAM-15 wt % in gel (G), oven-dried (D), and aerogel (A) forms. At first glance, as seen in Figure 11, a direct correlation emerges between the swelling temperature and swelling ratios. The SR exhibited a 60% increase at elevated temperature for the gel sample form compared with the SR at 25 °C. A more pronounced temperature effect was observed for the PAM-15 wt % in both oven-dried (D) and aerogel (A) sample forms, where SR of the oven-dried (D) and aerogel (A) increased by 90 and 20%, respectively, at 80 °C. Commonly, higher temperatures encourage the expansion of polymer chains, leading to an increase in SR. However, the disparity in SR between the oven-dried and freeze-dried samples is notable, with the aerogel sample demonstrating excellent water-absorbing capacity even at room temperature. Furthermore, we observed that the freeze-dried sample exhibited better structural stability at higher temperatures than the oven-dried sample.

Figure 12 shows the PAM-15 wt % hydrogel in aerogel form before and after swelling in pure water at 25 °C. Notably, the weight of the swollen aerogel sample increases by 83-fold compared to its dried state, achieved by immersing it in excess distilled water until it reaches an equilibrium swelling SR. To our knowledge, this value is the highest reported thus far for super-water-absorbent polymers.

Knowledge of the kinetic mechanism of the swelling process is paramount in hydrogel technology. Without a thorough understanding of how the swelling process occurs, it is impossible to design and develop effective hydrogels that can meet the specific needs of various applications. Therefore, it is imperative to delve deeper into the kinetics of the swelling

https://doi.org/10.1021/acsomega.4c00727
ACS Omega 2024, 9, 23531−23541

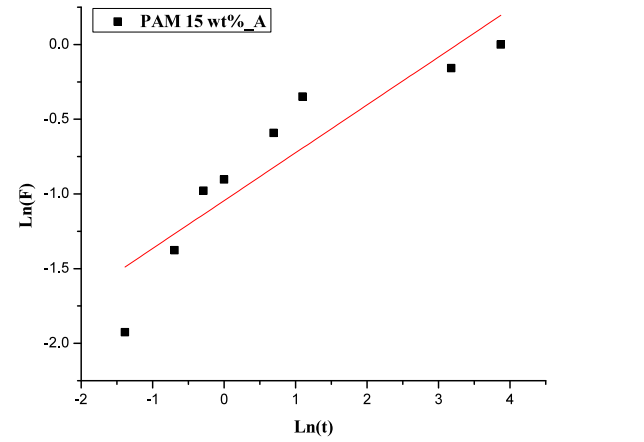

Sample Name	Initial Regression Equation	R^2	n	ln(k)
PAM 15 wt%_Freeze-dried (A)	Ln(F)=(0.32038)ln(t)+(-1.04476)	0.81147	0.32038	-1.04476

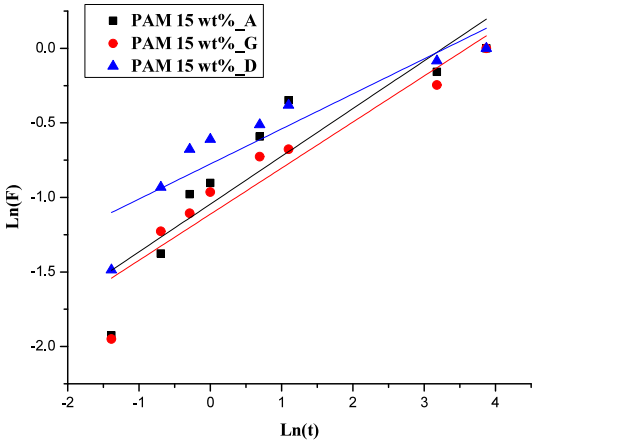

Sample Name	Initial Regression Equation	R^2	n	ln(k)
PAM 15 wt%_Hydrogel (G)	Ln(F)=(0.32038)ln(t)+(-1.04476)	0.81147	0.32038	-1.04476
PAM 15 wt%_Oven-dried (D)	Ln(F)=(0.30912)ln(t)+(-1.11262)	0.87848	0.30912	-1.11262
PAM 15 wt%_Freeze-dried (A)	Ln(F)=(0.23511)ln(t)+(-0.77572)	0.81344	0.23511	-0.77572

Figure 13. Curves of $\ln(t)$ vs $\ln(F)$ of PAM-15 wt % hydrogels at different drying methods in deionized water at 25 °C.

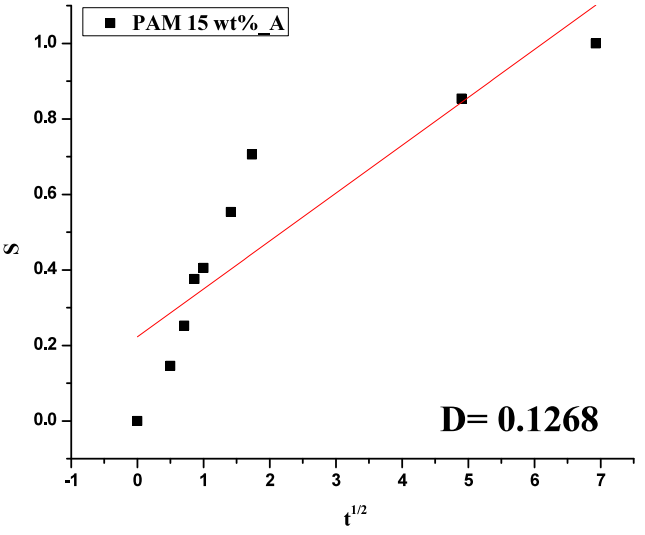

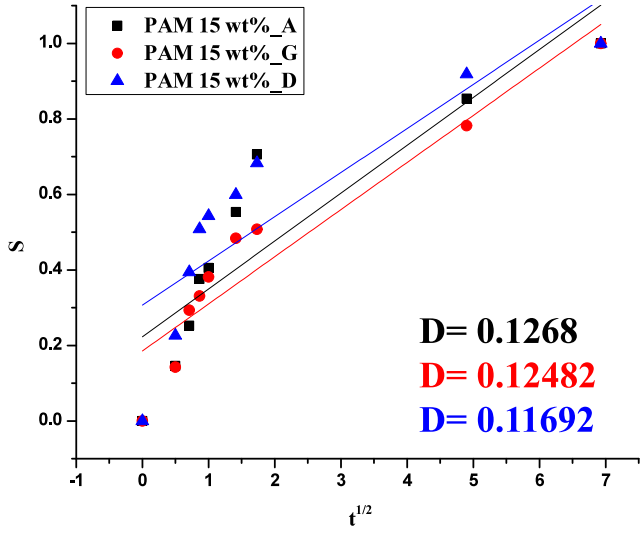

Figure 14. Curves of S vs $t^{1/2}$ of PAM-15 wt % hydrogels at different drying methods in deionized water at 25 °C.

process to harness the hydrogel technology's full potential. Typically, hydrogel swelling involves penetration of water into the voids of the hydrogel, leading to the expansion of polymeric chains.

Numerous techniques have been reported in the literature to study the swelling mechanism, and among them, a simple Fickian diffusion model is applied as expressed in eqs 5−7:

$$\ln(F) = n\ln(t) + \ln(k) \tag{5}$$

$$F = \frac{S_t}{S_{eq}} \tag{6}$$

$$\mathrm{SR} = \frac{\text{dried weight} - \text{swollen wieght}}{\text{dried weight}} \tag{7}$$

where F symbolizes the water fraction at time t; S_t and S_{eq} denote SR at time t (h) and equilibrium SR, respectively; t stands for the swelling time; K refers to the swelling rate constant; and n represents the diffusional/swelling exponent, which indicates the water transport mechanism. The constants n and k are calculated based on the slopes and intercepts derived from the $\ln(F)$ graph against $\ln(t)$ for PAM-15 wt % aerogel in distilled water at 25 °C.

Four distinct diffusion mechanism types are identified based on the n values. The first, where $n \leq 0.5$, signifies Fickian diffusion, where water transport primarily relies on a simple concentration gradient. The second, with $0.5 < n < 1.0$, corresponds to non-Fickian diffusion or anomalous diffusion, indicating that both diffusion and relaxation are equally effective. When $n = 1.0$, it represents Case II diffusion, where diffusion occurs rapidly, contrasting with the relaxation rate. The fourth, when $n > 1.0$ (rarely occurs), is attributed to the super Case II diffusion mechanism.

To determine the diffusion mechanism mode observed in our samples, a plot of $\ln(t)$ vs $\ln(F)$ was generated, and the slope of the resulting straight lines provided the swelling exponent value n. As depicted in Figure 13, the curve of $\ln(t)$ vs $\ln(F)$ exhibited a linear fit with a strong linear correlation coefficient ($R^2 = 0.81$). Based on the results from Figure 13, the swelling kinetics behaviors of PAM-15 wt % aerogel align

https://doi.org/10.1021/acsomega.4c00727
ACS Omega 2024, 9, 23531−23541

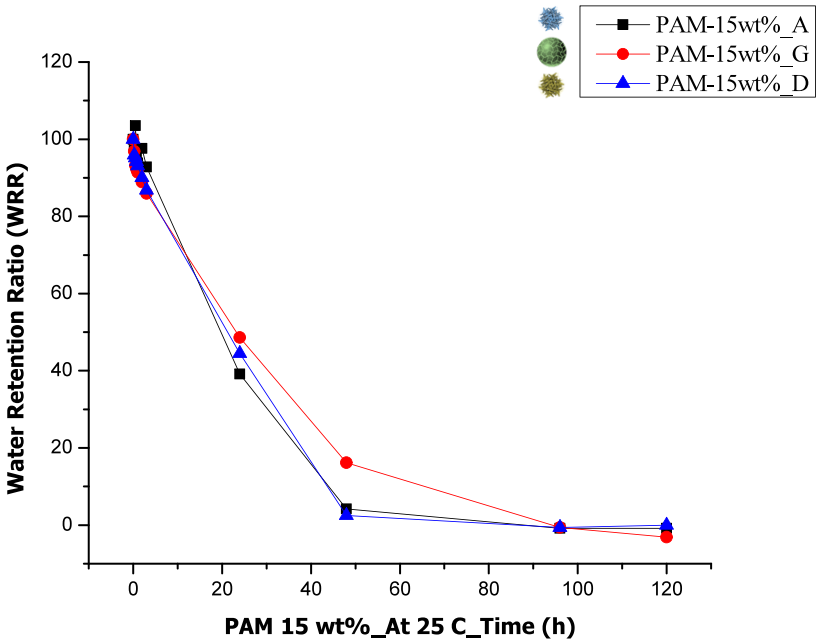

Figure 15. Water retention of PAM-15 wt % hydrogels with different drying methods in the open air at 25 °C.

with a Fickian-mode diffusion mechanism, where n is found to be ≤0.5. Such behavior indicates Fickian diffusion, a mode particularly suited for controlled release applications.

To analyze the diffusion rate concerning the kinetic model of PAM-15 wt % hydrogels, the diffusion coefficient value D was determined by plotting S vs $t_{1/2}$ (Figure 14), where the slope of the line provides the diffusion coefficient value. As depicted, the diffusion coefficient values for PAM-15 wt % hydrogels in both gel and freeze-dried forms were quite similar at 0.1248 and 0.1268 $cm^2 \cdot s^{-1}$, respectively. Conversely, the oven-dried form measured at 0.1169 $cm^2 \cdot s^{-1}$ indicated a comparatively faster diffusion rate of water molecules in the gel and freeze-dried forms compared with the oven-dried counterparts. These findings align with the outcomes obtained from DSC, as depicted in Figure 17, which suggested a lower degree of structural order in the entropy value of the oven-dried samples.

3.8. Deswelling. After attaining the equilibrium swelling of the PAM-15 wt % hydrogel in its various forms at 25 °C, they were reused in a subsequent water retention experiment. The water retention capability of these swollen PAM-15 wt % samples was assessed in an open-air setting at room temperature. As depicted in Figure 15, an extended water release was observed for up to 4 days, accompanied by a water retention ratio (WRR) of approximately 40% after 1 day in the open air, showcasing commendable water retention abilities.

3.9. Recyclability. Sequential swelling/deswelling experiments in distilled water were conducted to evaluate the recyclability of PAM-15 wt % in aerogel form, as illustrated in Figure 16. Initially, the freeze-dried PAM-15 wt % sample was immersed in excess distilled water to reach its equilibrium swelling. Subsequently, the swollen hydrogel sample was extracted from the water and dried to a constant weight at 50 °C. This drying cycle was repeated ten times, alternating with swelling in water. Even after 10 cycles, the SR remained consistently high, indicating an exceptional reswelling capability of this SAH sample. This remarkable recyclability can be attributed to its well-interconnected structures and robust framework, contributing to its enduring performance across multiple cycles.

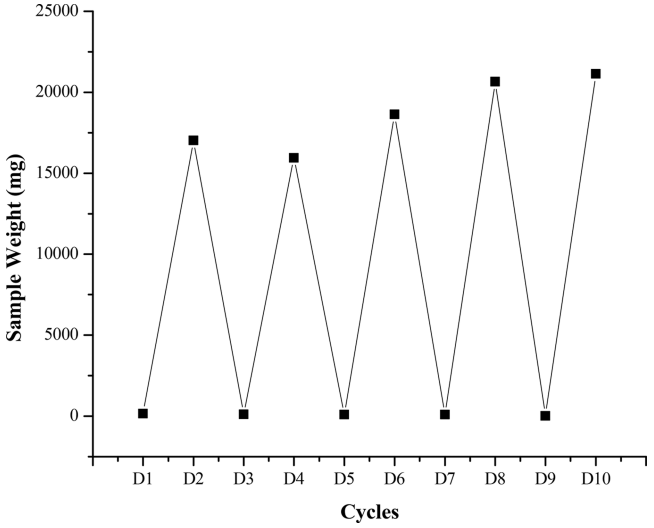

Figure 16. Recyclability of PAM-15 wt % hydrogels.

3.10. Mechanism. To evaluate the drying process effect on the hydrogel network from a thermodynamic perspective, DSC analysis was conducted, and corresponding parameters were derived. In Figure 17, the DSC curve of the oven-dried sample reveals a distinct endothermic peak around 50 °C, with an enthalpy value of ΔH = 3.6 J/g. This distinct peak suggests that the drying process induces structural alterations in the gel, potentially indicating structural collapse.

To determine disorder stability, the entropy ΔS was calculated as $\Delta H/T$, as detailed in the table in Figure 17. The entropy value indicates that the hydrogel post-oven-drying exhibited lower orderliness, likely attributed to the drying temperature, in contrast to the hydrogel before drying. Thus, it demonstrates that the freeze-drying method yields a more robust and stable structure compared to the oven-dried method.

https://doi.org/10.1021/acsomega.4c00727
ACS Omega 2024, 9, 23531−23541

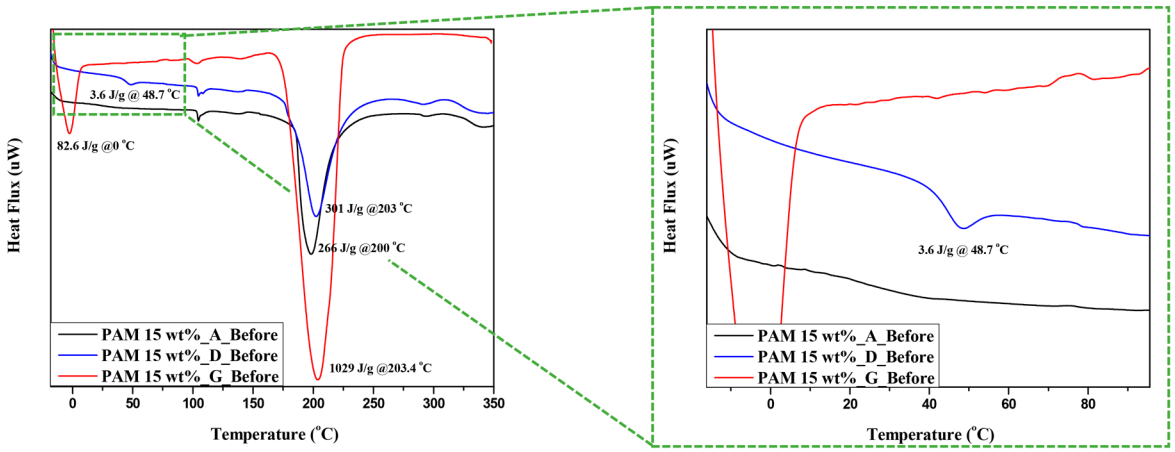

	H_{deg} (J/g)	T_{deg} (°C)
PAM 15 wt%_Hydrogel (G)	1029	203.4
PAM 15 wt%_Oven-dried (D)	301	203.0
PAM 15 wt%_Freeze-dried (A)	266	200.0

	Hydrogel (G)	Oven-dried (D)	Freeze-dried (A)
Temperature (°C)	-	48.7	-
ΔH (J/g)	-	3.6	-
ΔS* (J/g^{-1} °C^{-1})	-	0.07	-

*ΔS, calculated as ΔH/T

Figure 17. DSC thermograms of PAM-15 wt % hydrogels at different drying methods.

4. CONCLUSION

In conclusion, innovative SAHs were synthesized based on polyacrylamide (PAM) polymer, which features a three-dimensional structure. They can absorb and retain significant water volumes even under extreme environmental conditions, such as high temperatures and pressure, while retaining their original form. The results exhibited elevated levels of both SR and WRR, with the highest reported SR value exceeding 10000 wt % and remarkable WRR capability, which are very essential for agricultural applications. Notably, the freeze-dried hydrogel sample exhibited an 83-fold increase in weight after immersion in distilled water to reach equilibrium at room temperature. The application of these hydrogels holds promise in augmenting the water retention capabilities of sandy soils, potentially fostering agricultural activities in desert regions. Their exceptional water-absorbing properties could significantly benefit such environments.

AUTHOR INFORMATION

Corresponding Author

Edreese Alsharaeh − *Alfaisal University, College of Science, Chemistry Department, Riyadh 11533, Saudi Arabia;* orcid.org/0000-0002-3707-7883; Email: ealsharaeh@alfaisal.edu

Author

Haneen Omar − *Alfaisal University, College of Science, Chemistry Department, Riyadh 11533, Saudi Arabia;* orcid.org/0000-0003-1036-0387

Complete contact information is available at: https://pubs.acs.org/10.1021/acsomega.4c00727

Notes

The authors declare no competing financial interest.

ACKNOWLEDGMENTS

The authors extend their sincere appreciation to Mr. Attallah AlSlami and Mr. Abdullah K. Alshamari from King Abdulaziz City for Science and Technology (KACST) for the TGA characterizations, Mr. Yaser A. Butt from JEOL Co. for the SEM characterization, and Mr. Khalid Ahmed form Alfaisal University for the nanoindentation characterization.

REFERENCES

(1) Borrelli, P.; Robinson, D. A.; Fleischer, L. R.; Lugato, E.; Ballabio, C.; Alewell, C.; Meusburger, K.; Modugno, S.; Schütt, B.; Ferro, V.; Bagarello, V.; Oost, K. V.; Montanarella, L.; Panagos, P. An assessment of the global impact of 21st century land use change on soil erosion. *Nat. Commun.* **2017**, *8* (1), 2013.

(2) Amundson, R.; Berhe, A. A.; Hopmans, J. W.; Olson, C.; Sztein, A. E.; Sparks, D. L. J. S. Soil and human security in the 21st century. *Science* **2015**, *348* (6235), No. 1261071.

(3) Oladosu, Y.; Rafii, M. Y.; Arolu, F.; Chukwu, S. C.; Salisu, M. A.; Fagbohun, I. K.; Muftaudeen, T. K.; Swaray, S.; Haliru, B. S. Superabsorbent Polymer Hydrogels for Sustainable Agriculture: A Review. *Horticulture* **2022**, *8* (7), 605.

(4) Qin, C.-C.; Abdalkarim, S. Y. H.; Zhou, Y.; Yu, H.-Y.; He, X. Ultrahigh water-retention cellulose hydrogels as soil amendments for early seed germination under harsh conditions. *J. Clean. Prod.* **2022**, *370*, No. 133602.

(5) Gao, G.; Du, G.; Cheng, Y.; Fu, J. Tough nanocomposite double network hydrogels reinforced with clay nanorods through covalent bonding and reversible chain adsorption. *J. Mater. Chem. B* **2014**, *2* (11), 1539−1548.

(6) Wei, Y.; Durian, D. J. Rain water transport and storage in a model sandy soil with hydrogel particle additives. *Eur. Phys. J. E* **2014**, *37*, 97.

(7) Yang, L.; Yang, Y.; Chen, Z.; Guo, C.; Li, S. Influence of super absorbent polymer on soil water retention, seed germination and plant survivals for rocky slopes eco-engineering. *Ecol. Eng.* **2014**, *62*, 27−32.

(8) Xu, S.; Zhang, L.; McLaughlin, N. B.; Mi, J.; Chen, Q.; Liu, J. Effect of synthetic and natural water absorbing soil amendment soil physical properties under potato production in a semi-arid region. *Soil Tillage Res.* **2015**, *148*, 31−39.

(9) Bauli, C. R.; Lima, G. F.; de Souza, A. G.; Ferreira, R. R.; Rosa, D. S. Eco-friendly carboxymethyl cellulose hydrogels filled with nanocellulose or nanoclays for agriculture applications as soil conditioning and nutrient carrier and their impact on cucumber growing. *Colloids Surf., A* **2021**, *623*, No. 126771.

(10) Mandal, U. K.; Sharma, K.L.; Venkanna, K.; Korwar, G.R.; Reddy, K.S.; Pushpanjali; Reddy, N.N.; Venkatesh, G.; Masane, R. N.;

https://doi.org/10.1021/acsomega.4c00727
ACS Omega 2024, 9, 23531−23541

Yadaiah, P. Evaluating hydrogel application on soil water availability and crop productivity in semiarid tropical red soil. *Indian J. Dryland Agric. Res. Dev.* **2015**, *30* (2), 1−10.
(11) Thombare, N.; Mishra, S.; Siddiqui, M.; Jha, U.; Singh, D.; Mahajan, G. R. J. C. p. Design and development of guar gum based novel, superabsorbent and moisture retaining hydrogels for agricultural applications. *Carbohydr. Polym.* **2018**, *185*, 169−178.
(12) Ma, X.; Wen, G. Development history and synthesis of superabsorbent polymers: a review. *J. Polym. Res.* **2020**, *27* (6), 136.
(13) Zohuriaan-Mehr, M. J.; Kabiri, K. Superabsorbent polymer materials: a review. *Iran. Polym. J.* **2008**, *17* (6), 451−477.
(14) Peppas, N. A.; Merrill, E. W. Crosslinked poly (vinyl alcohol) hydrogels as swollen elastic networks. *J. Appl. Polym. Sci.* **1977**, *21* (7), 1763−1770.
(15) Liu, M.; Liang, R.; Zhan, F.; Liu, Z.; Niu, A. Preparation of superabsorbent slow release nitrogen fertilizer by inverse suspension polymerization. *Polym. Int.* **2007**, *56* (6), 729−737.
(16) Lim, D.-W.; Song, K.-G.; Yoon, K.-J.; Ko, S.-W. J. Synthesis of acrylic acid-based superabsorbent interpenetrated with sodium PVA sulfate using inverse-emulsion polymerization. *Eur. Polym. J.* **2002**, *38* (3), 579−586.
(17) Liu, Z. S.; Rempel, G. L. Preparation of superabsorbent polymers by crosslinking acrylic acid and acrylamide copolymers. *J. Appl. Polym. Sci.* **1997**, *64* (7), 1345−1353.
(18) Zohuriaan-Mehr, M.; Omidian, H.; Doroudiani, S.; Kabiri, K. Advances in non-hygienic applications of superabsorbent hydrogel materials. *J. Mater. Sci.* **2010**, *45*, 5711−5735.
(19) Oladosu, Y.; Rafii, M. Y.; Arolu, F.; Chukwu, S. C.; Salisu, M. A.; Fagbohun, I. K.; Muftaudeen, T. K.; Swaray, S.; Haliru, B. S. J. H. Superabsorbent polymer hydrogels for sustainable agriculture: A review. *Horticulture* **2022**, *8* (7), 605.
(20) Venkatachalam, D.; Kaliappa, S. Superabsorbent polymers: A state-of-art review on their classification, synthesis, physicochemical properties, and applications. *Rev. Chem. Eng.* **2023**, *39* (1), 127−171.
(21) Djafari Petroudy, S. R.; Ranjbar, J.; Rasooly Garmaroody, E. Eco-friendly superabsorbent polymers based on carboxymethyl cellulose strengthened by TEMPO-mediated oxidation wheat straw cellulose nanofiber. *Carbohydr. Polym.* **2018**, *197*, 565−575.
(22) Bhardwaj, A. K.; Shainberg, I.; Goldstein, D.; Warrington, D. N.; Levy, G. J. Water Retention and Hydraulic Conductivity of Cross-Linked Polyacrylamides in Sandy Soils. *Soil Sci. Soc. Am. J.* **2007**, *71* (2), 406−412.
(23) Kiran; Tiwari, R.; Krishnamoorthi, S.; Kumar, K. Synthesis of cross-linker devoid novel hydrogels: Swelling behaviour and controlled urea release studies. *J. Environ. Chem. Eng.* **2019**, *7* (4), No. 103162.
(24) Hong, T. T.; Okabe, H.; Hidaka, Y.; Hara, K. Radiation synthesis and characterization of super-absorbing hydrogel from natural polymers and vinyl monomer. *Environ. Pollut.* **2018**, *242*, 1458−1466.
(25) Lv, Q.; Wu, M.; Shen, Y. Enhanced swelling ratio and water retention capacity for novel super-absorbent hydrogel. *Colloids Surf., A* **2019**, *583*, No. 123972.
(26) Krishnan, M. R.; Alsharaeh, E. H. Polymer gel amended sandy soil with enhanced water storage and extended release capabilities for sustainable desert agriculture. *J. Polym. Sci. Eng.* **2023**, *6* (1), 2892.
(27) Yang, Z. L.; Gao, B. Y.; Li, C. X.; Yue, Q. Y.; Liu, B. Synthesis and characterization of hydrophobically associating cationic polyacrylamide. *Chem. Eng. J.* **2010**, *161* (1), 27−33.
(28) Zhong, C.; Huang, R.; Xu, J. Characterization, solution behavior, and microstructure of a hydrophobically associating nonionic copolymer. *J. Solution Chem.* **2008**, *37*, 1227−1243.
(29) Zhang, X.; Han, M.; Xu, L.; AlSofi, A. M. Long-term stability prediction of polyacrylamide-type polymers at harsh conditions via thermogravimetric analysis. *Chem. Phys. Lett.* **2022**, *795*, No. 139538.

https://doi.org/10.1021/acsomega.4c00727
ACS Omega 2024, 9, 23531−23541